Wideband optical sensing using pulse interferometry

Amir Rosenthal,* Daniel Razansky, and Vasilis Ntziachristos

Institute for Biological and Medical Imaging (IBMI), Technical University of Munich and Helmholtz Center Munich, IngoldstädterLandstraße 1, 85764 Neuherberg, Germany

*eeamir@mytum.de

Abstract: Advances in fabrication of high-finesse optical resonators hold promise for the development of miniaturized, ultra-sensitive, wide-band optical sensors, based on resonance-shift detection. Many potential applications are foreseen for such sensors, among them highly sensitive detection in ultrasound and optoacoustic imaging. Traditionally, sensor interrogation is performed by tuning a narrow linewidth laser to the resonance wavelength. Despite the ubiquity of this method, its use has been mostly limited to lab conditions due to its vulnerability to environmental factors and the difficulty of multiplexing – a key factor in imaging applications. In this paper, we develop a new optical-resonator interrogation scheme based on wideband pulse interferometry, potentially capable of achieving high stability against environmental conditions without compromising sensitivity. Additionally, the method can enable multiplexing several sensors. The unique properties of the pulse-interferometry interrogation approach are studied theoretically and experimentally. Methods for noise reduction in the proposed scheme are presented and experimentally demonstrated, while the overall performance is validated for broadband optical detection of ultrasonic fields. The achieved sensitivity is equivalent to the theoretical limit of a 6 MHz narrow-line width laser, which is 40 times higher than what can be usually achieved by incoherent interferometry for the same optical resonator.

OCIS codes: (280.4788) Optical sensing and sensors; (120.3180) Interferometry; (060.3735) Fiber Bragg gratings; (320.5550) Pulses.

References and links

1. A. A. Michelson and E. W. Morley, "On the relative motion of the earth and the luminiferous ether," Am. J. Sci. **34**, 333–345 (1887).
2. A. D. Kersey, M. A. Davis, H. J. Patrick, M. LeBlanc, K. P. Koo, C. G. Askins, M. A. Putnam, and E. J. Friebele, "Fiber grating sensor," J. Lightwave Technol. **15**(8), 1442–1463 (1997).
3. J. A. Bucaro, H. D. Dardy, and E. F. Carome, "Fiber-optic hydrophone," J. Acoust. Soc. Am. **62**(5), 1302–1304 (1977).
4. T. T. Y. Lam, G. Gagliardi, M. Salza, J. H. Chow, and P. De Natale, "Optical fiber three-axis accelerometer based on lasers locked to π phase-shifted Bragg gratings," Meas. Sci. Technol. **21**(9), 094010 (2010).
5. C. Fabry and A. Pérot, "On the fringes of thin silver plates and their application to the measurement of small layers of air," Ann. Chim. Phys. **12**, 459–501 (1897).
6. S. John, "Strong localization of photons in certain disordered dielectric superlattices," Phys. Rev. Lett. **58**(23), 2486–2489 (1987).
7. B. E. Little, S. T. Chu, H. A. Haus, J. Foresi, and J. P. Laine, "Microring resonator channel dropping filters," J. Lightwave Technol. **15**(6), 998–1005 (1997).
8. K. O. Hill, Y. Fujii, D. C. Johnson, and B. S. Kawasaki, "Photosensitivity in optical fiber waveguides: application to reflection fiber fabrication," Appl. Phys. Lett. **32**(10), 647–649 (1978).
9. Y. Akahane, T. Asano, B. S. Song, and S. Noda, "High-Q photonic nanocavity in a two-dimensional photonic crystal," Nature **425**(6961), 944–947 (2003).
10. A. Rosenthal, D. Razansky, and V. Ntziachristos, "High-sensitivity compact ultrasonic detector based on a pi-phase-shifted fiber Bragg grating," Opt. Lett. **36**(10), 1833–1835 (2011).

#167037 - $15.00 USD Received 18 Apr 2012; revised 25 Jun 2012; accepted 27 Jun 2012; published 3 Aug 2012

11. D. Gallego and H. Lamela, "High-sensitivity ultrasound interferometric single-mode polymer optical fiber sensors for biomedical applications," Opt. Lett. **34**(12), 1807–1809 (2009).
12. P. Morris, A. Hurrell, A. Shaw, E. Zhang, and P. Beard, "A Fabry-Perot fiber-optic ultrasonic hydrophone for the simultaneous measurement of temperature and acoustic pressure," J. Acoust. Soc. Am. **125**(6), 3611–3622 (2009).
13. E. Zhang, J. Laufer, and P. Beard, "Backward-mode multiwavelength photoacoustic scanner using a planar Fabry-Perot polymer film ultrasound sensor for high-resolution three-dimensional imaging of biological tissues," Appl. Opt. **47**(4), 561–577 (2008).
14. S. W. Huang, S. L. Chen, T. Ling, A. Maxwell, M. O'Donnell, L. J. Guo, and S. Ashkenazi, "Low-noise wideband ultrasound detection using polymer microring resonators," Appl. Phys. Lett. **92**(19), 193509 (2008).
15. T. Ling, S. L. Chen, and L. J. Guo, "Fabrication and characterization of high Q polymer micro-ring resonator and its application as a sensitive ultrasonic detector," Opt. Express **19**(2), 861–869 (2011).
16. D. Razansky, M. Distel, C. Vinegoni, R. Ma, N. Perrimon, R. W. Köster, and V. Ntziachristos, "Going deeper than microscopy with multi-spectral optoacoustic tomography of fluorescent proteins in-vivo," Nat. Photonics **3**, 412–417 (2009).
17. V. Ntziachristos and D. Razansky, "Molecular imaging by means of multispectral optoacoustic tomography (MSOT)," Chem. Rev. **110**(5), 2783–2794 (2010).
18. D. Razansky, A. Buehler, and V. Ntziachristos, "Volumetric real-time multispectral optoacoustic tomography of biomarkers," Nat. Protoc. **6**(8), 1121–1129 (2011).
19. D. Razansky, S. Kellnberger, and V. Ntziachristos, "Near-field radiofrequency thermoacoustic tomography with impulse excitation," Med. Phys. **37**(9), 4602–4607 (2010).
20. B. Lissak, A. Arie, and M. Tur, "Highly sensitive dynamic strain measurements by locking lasers to fiber Bragg gratings," Opt. Lett. **23**(24), 1930–1932 (1998).
21. J. H. Chow, I. C. M. Littler, D. E. Glenn de Vine, D. E. McClelland, and M. B. Gray, "Phase-sensitive interrogation of fiber Bragg grating resonators for sensing applications," J. Lightwave Technol. **23**(5), 1881–1889 (2005).
22. J. H. Chow, I. C. Littler, D. E. McClelland, and M. B. Gray, "Laser frequency-noise-limited ultrahigh resolution remote fiber sensing," Opt. Express **14**(11), 4617–4624 (2006).
23. J. H. Chow, D. E. McClelland, M. B. Gray, and I. C. M. Littler, "Demonstration of a passive subpicostrain fiber strain sensor," Opt. Lett. **30**(15), 1923–1925 (2005).
24. G. Gagliardi, M. Salza, S. Avino, P. Ferraro, and P. De Natale, "Probing the ultimate limit of fiber-optic strain sensing," Science **330**(6007), 1081–1084 (2010).
25. T. T. Y. Lam, J. H. Chow, D. A. Shaddock, I. C. M. Littler, G. Gagliardi, M. B. Gray, and D. E. McClelland, "High-resolution absolute frequency referenced fiber optic sensor for quasi-static strain sensing," Appl. Opt. **49**(21), 4029–4033 (2010).
26. S. Avino, J. A. Barnes, G. Gagliardi, X. Gu, D. Gutstein, J. R. Mester, C. Nicholaou, and H. P. Loock, "Musical instrument pickup based on a laser locked to an optical fiber resonator," Opt. Express **19**(25), 25057–25065 (2011).
27. C. K. Kirkendall and A. Dandridge, "Overview of high performance fiber-optic sensing," J. Phys. D Appl. Phys. **37**(18), R197–R216 (2004).
28. G. A. Cranch, P. J. Nash, and C. K. Kirkendall, "Large-scale remotely interrogated arrays of fiber-optic interferometric sensors for underwater acoustic applications," IEEE Sens. J. **3**(1), 19–30 (2003).
29. I. C. M. Littler, M. B. Gray, J. H. Chow, D. A. Shaddock, and D. E. McClelland, "Pico-strain multiplexed fiber optic sensor array operating down to infra-sonic frequencies," Opt. Express **17**(13), 11077–11087 (2009).
30. M. A. Yaseen, S. A. Ermilov, H. P. Brecht, R. Su, A. Conjusteau, M. Fronheiser, B. A. Bell, M. Motamedi, and A. A. Oraevsky, "Optoacoustic imaging of the prostate: development toward image-guided biopsy," J. Biomed. Opt. **15**(2), 021310 (2010).
31. A. D. Kersey, D. A. Jackson, and M. Corke, "Passive compensation scheme suitable for use in the single-mode fiber interferometer," Electron. Lett. **18**(9), 392–393 (1982).
32. A. D. Kersey, M. A. Davis, H. J. Patrick, M. LeBlanc, K. P. Koo, C. G. Askins, M. A. Putnam, and E. J. Friebele, "Fiber grating sensors," J. Lightwave Technol. **15**(8), 1442–1463 (1997).
33. A. T. Alavie, S. E. Karr, A. Othonos, and R. M. Measures, "A multiplexed Bragg grating fiber laser sensor system," IEEE Photon. Technol. Lett. **5**(9), 1112–1114 (1993).
34. G. A. Cranch, G. M. H. Flockhart, and C. K. Kirkendall, "Distributed feedback fiber laser strain sensor," IEEE Sens. J. **8**(7), 1161–1172 (2008).
35. K. P. Koo and A. D. Kersey, "Fiber laser sensor with ultrahigh strain resolution using interferometric interrogation," Electron. Lett. **31**(14), 1180–1182 (1995).
36. L. Y. Shao, S. T. Lau, X. Dong, A. P. Zhang, H. L. W. Chan, H. Y. Tam, and S. He, "High-frequency ultrasonic hydrophone based on a cladding-etched DBR fiber laser," IEEE Photon. Technol. Lett. **20**(8), 548–550 (2008).
37. C. C. Ye and R. P. Tatam, "Ultrasonic sensing using Yb3+/Er3+-codoped distributed feedback fiber grating lasers," Smart Mater. Struct. **14**(1), 170–176 (2005).
38. B. Moslehi, "Noise power spectra of optical two-beam interferometers induced by the laser phase noise," J. Lightwave Technol. **4**(11), 1704–1710 (1986).
39. G. Di Domenico, S. Schilt, and P. Thomann, "Simple approach to the relation between laser frequency noise and laser line shape," Appl. Opt. **49**(25), 4801–4807 (2010).

#167037 - $15.00 USD Received 18 Apr 2012; revised 25 Jun 2012; accepted 27 Jun 2012; published 3 Aug 2012

40. D. Gatti, G. Galzerano, D. Janner, S. Longhi, and P. Laporta, "Fiber strain sensor based on a pi-phase-shifted Bragg grating and the Pound-Drever-Hall technique," Opt. Express **16**(3), 1945–1950 (2008).
41. D. A. Jackson, R. Priest, A. Dandridge, and A. B. Tveten, "Elimination of drift in a single-mode optical fiber interferometer using a piezoelectrically stretched coiled fiber," Appl. Opt. **19**(17), 2926–2929 (1980).
42. R. S. Weis and B. L. Bachim, "Source-noise-induced resolution limits of interferometric fiber Bragg grating sensor demodulation systems," Meas. Sci. Technol. **12**(7), 782–785 (2001).
43. T. Erdogan, "Fiber grating spectra," J. Lightwave Technol. **15**(8), 1277–1294 (1997).

1. Introduction

Optical interferometry has been used for over a century to measure optical-path variations [1–3] and comprises the principle of operation for many optical sensors for sensing physical quantities such as temperature [2], pressure [2], sound [3], and acceleration [4]. Improvements in interferometric sensors have been achieved using optical cavities, which trap light, thus amplifying the accumulated phase over a certain distance [4–10]. Advances in the fabrication of optical devices have led to cavities with high quality factors which enable efficient capturing of light over short distances [7, 9, 10]. Additionally, resonators with narrow notches may be produced in fibers, e.g. in π-phase-shifted fiber Bragg gratings (FBG) [4, 10], or fiber-coupled devices, thus enabling remote sensing.

In recent years, the application of interferometric sensors for ultrasound detection has attracted considerable attention [10–15]. One of the promising applications currently being researched is the use of such sensor for biomedical imaging, namely optoacoustic and radio frequency thermoacoustic imaging [16–19], where piezoelectric sensors are commonly employed. In optoacoustic imaging, where laser light leads to the formation of ultrasound waves via local heating and thermal expansion [16], the transparency of optical detectors has been shown to enable new designs [13] while miniaturization of the detectors could enable catheter- and endoscope-based implementations [10, 12]. In thermoacoustic imaging, where ultrasound is created by applying high-power electromagnetic fields to the imaged object, the immunity of optical detection of ultrasound to electromagnetic interference may also greatly improve imaging fidelity.

In order to use high-finesse optical resonators as sensors, appropriate methods for monitoring variations in their resonance wavelength are required. This is typically achieved by tuning a continuous wave (CW) narrow-linewidth laser beam to the wavelength in which the resonance occurs and measuring the intensity of either the reflected or transmitted light [4, 10]. Cavity variations in terms of refractive index or geometry can shift the resonance wavelength, which is translated into a change in the monitored intensity. By locking the laser's wavelength to that of the resonator, a wide dynamic range may be achieved for the optical sensor [4, 20 ,21]. When the Pound-Drever-Hall (PDH) frequency-locking technique is used, frequency-noise-limited detection may be achieved [22, 23]. PHD-based sensing techniques have been extremely successful in detecting low-frequency vibrations from sub-Hertz nanostrains [24, 25] to audio frequencies up to 20 kHz [26] and could also be potentially used for the detection of ultrasound. One of the major hurdles in the practical application of PDH-based sensing is the difficulty in stabilizing the laser to the resonator in the presence of strong perturbations. Recently, stable performance under strains of up to 1-2 με have been demonstrated using the PDH method, which enabled its use for musical instrument pickup [26]. Nonetheless, the upper limit on the dynamic range of the PDH method might limit its application in more volatile environments.

A more fundamental limitation of narrow-linewidth interrogation for imaging is the challenge of parallel multiplexing. When the optical sensor is an interferometer with a sinusoidal spectrum, techniques such as frequency division multiplexing [27] and time division multiplexing [27, 28] may enable interrogating many sensors with a single laser. However, when the sensor is an optical resonator which requires that the laser be locked to its wavelength, simultaneous interrogation is only possible when the number of lasers employed is equal to that of the resonators interrogated. Recently, multiplexed interrogation of four resonators has been demonstrated using PDH with four lasers using wavelength division multiplexing [29]. Although this approach may be used for multiplexing a larger number of resonators, its cost would scale linearly with the number resonators, which may prohibit applications in ultrasound sensing, where piezoelectric ultrasound arrays with over 100 elements are commonplace [30].

An alternative interrogation method is based on using wideband incoherent CW sources [2]. The advantage of this method is that resonance frequencies of the interrogated device always fall within the source's band. Thus, no tuning of the source is required and stable operation may be achieved even under harsh environmental conditions if passive demodulation techniques are used [31]. Additionally, a single source may be used to simultaneously interrogate several resonators by using wavelength multiplexing [32].Moreover, using frequency-modulation techniques, multiplexing may be achieved with minimal scaling of the components [27]. However, the broad bandwidth of the source comes at an inherent price of high phase and amplitude noise, whose relative contribution to the measured noise increases with resonance strength. Thus, the use of such sources impedes incremental improvements in detection sensitivity when increasing the resonance strength. In addition, in many cases, such as π-phase-shifted FBGs or etalons, this technique can be used only in transmission, preventing sensor applications in which the sensing element is accessible from one side only, e.g. catheters or endoscopes.

One of the possible solutions for the deficiencies of CW interrogation methods are fiber laser sensors, in which the resonator is created in an active medium, enabling its operation as a laser. In such schemes, the active cavity is pumped by an external source which leads to lasing at the resonance wavelength, whereas variations in the resonance condition are measured by monitoring the wavelength shifts in the fiber laser output. Since this scheme does not require locking a laser to the resonator’s wavelength, efficient wavelength division multiplexing may be performed with only a single source, used for pumping. However, if the resonators are cascaded, significant crosstalk may occur as a result of optical feedback [33, 34]. Additionally, despite the high performance of fiber laser sensors in low-frequency sensing [35] or single-frequency ultrasound sensing [36], their use for detecting broadband ultrasound is severely limited by relaxation oscillations of the laser sensors [37]. Finally, the technique is limited to only resonator technologies which can be used in active media.

In this paper we propose a novel scheme for interrogating high-finesse optical resonators for sensing applications, which combines the benefits of wideband interrogation, namely stability and multiplexing capabilities, with high sensitivity. The method is based on using an interferometric setup with a wideband coherent pulsed source. The use of a wideband source opens the possibility for scalable multiplexing, similarly to previously demonstrated implementations applying low-coherence sources [2]. We further present a theoretical analysis of the suggested method, identifying several possible noise sources while an experimental demonstration is performed for ultrasound detection using a π-phase-shifted. In contrast to incoherent CW sources, in which the wide bandwidth is purely a result of a stochastic process, in coherent pulsed sources, the spectral span is a result of the deterministic shape of individual pulses. In our experiments, amplified spontaneous emission (ASE) was found to be the main source of noise. The achieved sensitivity was 18 times higher than that achieved with an incoherent-CW source used to interrogate the same resonator. By using a saturable absorber (SA) for ASE rejection, this factor was increased up to 40, a sensitivity level comparable to the theoretical limit achieved by narrow-linewidth interferometry using a 6 MHz linewidth CW laser.

Similarly to wideband incoherent CW interferometry, the natural implementation of pulse interferometry for resonators is in transmission mode. In order to enable operation in reflection mode, a new procedure of spectral inversion was developed. This procedure is based on destructively interfering the signal reflected from the resonator with a reference beam, thus transforming its spectral shape to that obtained in the transmission. The method is

#167037 - $15.00 USD Received 18 Apr 2012; revised 25 Jun 2012; accepted 27 Jun 2012; published 3 Aug 2012

demonstrated for π-phase-shifted FBGs, but can be applied to any resonator exhibiting a Lorenzian spectrum, e.g. etalons.

2. Theory

In this section we give a comparative analysis of coherent and incoherent CW interrogation techniques and pulse interferometry interrogation. The analysis is performed for Lorenzian shaped resonances, which are commonly found in optical resonators. We denote the central optical frequency of the resonance by υ_0 and its width by $\Delta\upsilon$. A qualitative comparison of the three methods is given in Fig. 1.

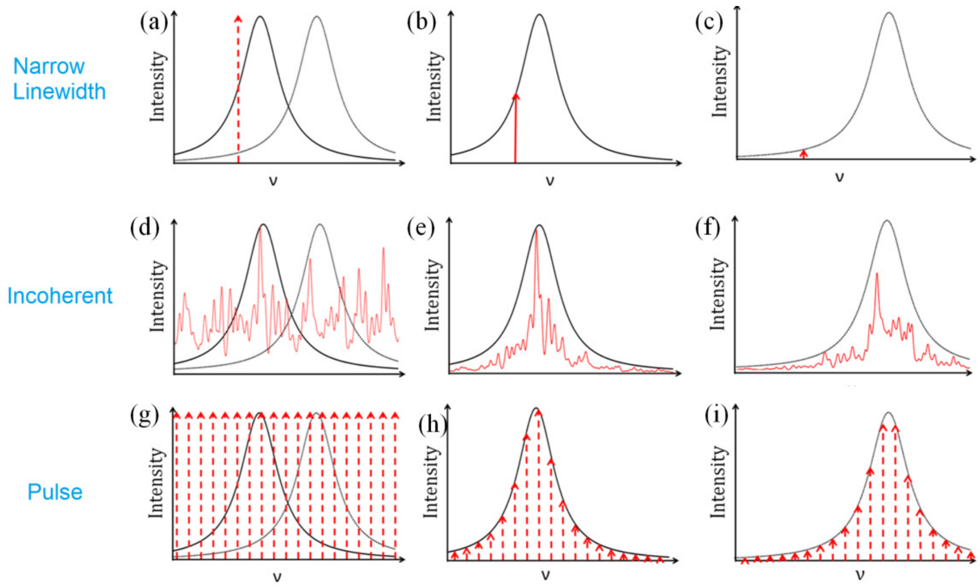

Fig. 1. A schematic description of (a-c) narrowband and (d-f) wideband CW interrogation and (g-i) wideband pulse interrogation of an optical bandpass filter. The first column shows the source's spectrum (red) and the resonance's spectrum for two possible central frequencies. The two additional columns show the spectrum of the source after passing through each of the respective resonance spectra.

2.1 Coherent CW interferometry

In coherent CW interrogation (Fig. 1(a)), the frequency of a narrow linewidth laser υ is often tuned to the point of maximum steepness in the resonance $(\nu - \nu_0 = \Delta\nu / 6)$ and the reflected or transmitted intensity is monitored [10, 12–15, 20]. As the resonance shifts, the monitored intensity changes (Figs. 1(b) and 1(c)). However, shifts that are larger than the width of the resonance can effectively saturate the measurement. Assuming that the central frequency shifts with a rate of $d\nu_0 / dt$, the normalized intensity will change with a maximum rate of $dI / (Idt) = (\sqrt{27} / 8) d\nu_0 / (\Delta\nu dt)$. In order to lock the laser wavelength to the resonance, e.g. using negative feedback, the tuning rate should exceed $dI / (Idt)$. As a result, the narrower the resonance, the faster the feedback response should be.

In coherent CW interrogation, the dominant process determining the noise is the conversion of phase noise into intensity noise [38]. The input field to the resonance is given by $u_{in}(t) = A\exp\{i[-2\pi i\nu t + \phi(t)]\}$, where $A = \sqrt{P_0}$ is the field's amplitude and $\phi(t)$ represents the phase noise. The frequency noise process, given by $f(t) = (2\pi)^{-1} d\phi(t) / dt$ is modeled by

#167037 - $15.00 USD Received 18 Apr 2012; revised 25 Jun 2012; accepted 27 Jun 2012; published 3 Aug 2012

white Gaussian noise with spectral density of $\Delta\nu_c/\pi$, where $\Delta\nu_c$ is the linewidth of the laser [39]. Denoting the measurement bandwidth by f and assuming $\Delta\nu_c, f \ll \Delta\nu$, a first-order Taylor expansion to the transmission function of the resonator $t_g(\nu)$ Eq. (8) around its maximum steepness may be used to calculate the power of the transmitted field, i.e.

$$\left|u_{\text{out}}(t)\right|^2 \cong P_0\left[\frac{3}{4}+\frac{\sqrt{27}}{8\Delta\nu}f(t)\right]. \tag{2}$$

The second term in Eq. (2) has a standard deviation of $P_{std} = P_0\sqrt{27\Delta\nu_c f}/(8\sqrt{\pi}\Delta\nu)$, leading to a signal-to-noise ratio of

$$\text{SNR}=\sqrt{\frac{\pi}{\Delta\nu_c f}}d\nu_0. \tag{3}$$

When phase noise is dominant, the SNR is independent of $\Delta\nu$. Thus, in this regime, counter-intuitively increasing the resonance strength does not increase the SNR. When phase noise is lower than other noise processes in the detection path, namely shot noise and sampling noise, sensitivity increases with $\Delta\nu$. However, in order to maintain the phase noise below a certain threshold for exceedingly narrower resonances, the laser linewidth $\Delta\nu_c$ must be scaled with $\Delta\nu^2$.

An alternative implementation of coherent CW interrogation consists of locking the laser to the extremum of the resonance using the PDH locking-scheme [4]. One of the major advantages of this approach is that it is insensitive to amplitude noise from the laser, making frequency-noise limited detection easier to achieve [22]. However, the tuning rate required to maintain the locked operation is still scaled with $\Delta\nu$. Additionally, despite the insensitivity of the PDH method to amplitude noise, the experimental evidence in Refs [4, 40]. shows that the effect of phase noise on its performance is governed by Eq. (3). Thus, despite its practical advantages, PDH has the same fundamental limit on its sensitivity as narrow-linewidth interrogation in which the laser is tuned to the linear part of the resonance. Finally, the use of PDH does not circumvent a fundamental challenge of multiplexing in coherent CW schemes: the number of lasers must be equal to the number of interrogated resonators [29].

2.2 Incoherent CW interferometry

Figure 1(d) illustrates wideband incoherent interrogation. The transmitted light assumes the spectral shape of the resonance (Figs. 1(e) and 1(f)) and its mean frequency is monitored, e.g. using a Mach-Zehnder (MZ) interferometer and demodulation, to detect resonance shifts [2]. Generally, demodulation may be performed either actively or passively. In active demodulation [36, 41], the interferometer is locked to a specific state for which its output is a linear function of the monitored resonance frequency. In passive demodulation [31], optical manipulation is applied to obtain two complementing outputs out of the interferometer which can be processed to monitor the resonance frequency without any locking mechanism. The ability to perform sensor interrogation without the need of a feedback-based compensation mechanism is an inherent advantage of incoherent CW interferometry over coherent CW interferometry and is a direct result of wideband illumination. However, in the case of incoherent CW interferometry, this comes at the cost of lower sensitivity. Because of the spectral distribution of the source's intensity is an inherently random process, the mean frequency of the transmitted light does not exactly coincide with that of the resonance, but rather fluctuates. These fluctuations, analyzed henceforth, pose an intrinsic limitation on the detection sensitivity.

#167037 - $15.00 USD Received 18 Apr 2012; revised 25 Jun 2012; accepted 27 Jun 2012; published 3 Aug 2012

The statistics of linearly polarized incoherent sources can be modeled by a Gaussian random process. Some of the noise properties of such sources were previously analyzed for a Gaussian spectral density [42]. In the case of a Lorentzian spectral density, and assuming $f \ll \Delta\nu$, the standard deviation of the power detected by the MZ interferometer is equal to $P_{\mathrm{std}} = P_0\sqrt{f/(2\pi\Delta\nu)}$ where P_0 is the source power. The visibility of the interferometer is given by $V = \exp(-|\pi\Delta\nu T|)$ where T is the delay between the interferometer arms. Assuming the interferometer is set to quadrature point, a shift in the central frequency of the Lorentzian $d\nu$ will cause the power to change by $P_{\mathrm{sig}} = P_0\pi\exp(-|\pi\Delta\nu T|)Td\nu$. The maximum SNR, obtained for $T = (\pi\Delta\nu)^{-1}$, is given by

$$\mathrm{SNR}=\sqrt{\frac{2\pi\Delta\nu}{e^2 f}}\frac{d\nu}{\Delta\nu}, \tag{4}$$

where $d\nu$ is the shift of the resonance's central frequency. Equation (4) elucidates the intrinsic limitation of the incoherent-wideband-interrogation method. When the measurement bandwidth is fixed, SNR is inversely proportional to $\sqrt{\Delta\nu}$, which limits the sensitivity improvements that can be achieved by using narrow resonance notches. Additionally, when the measurement is performed over a bandwidth approaching the resonance bandwidth, e.g. $f \approx 0.1\Delta\nu$, only resonance shifts comparable to $\Delta\nu$ or larger than it can be detected. Thus, for a given resonator, variations smaller than $\Delta\nu$ can only be detected by reducing the measurement bandwidth below its fundamental limit, which is a procedure equivalent to averaging in time. This property is illustrated in Figs. 1(d)-1(f), where the uncertainty in the mean frequency of the transmitted light is visible. The inability to detect variations smaller than the resonance width severely limits the incremental sensitivity gain which can be obtained from increasing the strength of the resonance in wideband CW techniques and make them significantly less sensitive than narrow-linewidth CW interrogation whose linewidth fulfills $\nu_c \ll \Delta\nu$.

2.3 Pulse interferometry

Herein we propose using pulsed lasers, which are both wideband and coherent. Such sources often exhibit a wideband comb structure in the spectral domain (Fig. 1(g)) with the spacing between the comb's teeth ν_s being equal to the repetition rate of the pulses. By passing through the resonance, the envelope of the comb takes up the form of the resonance spectrum, while detection can be performed by estimating the mean frequency of the resulting spectrum using the same techniques described in Section 2.2 for incoherent CW interferometry [31, 32, 41]. In the time domain, the laser pulses are broadened as a result of being convolved with the impulse response of the resonance. Thus, in order to assure that the mean frequencies of the resonance and of the filtered comb coincide, it is sufficient to impose that the broadened pulses of the source do not overlap, i.e. $\tau_g \ll \nu_s^{-1}$ where τ_g is the effective duration of the pulses at the output of the resonator. In such a case, the spectrum of each pulse approximates that of the resonance.

The field of a pulsed coherent source can be modeled via

$$u_{\mathrm{in}}(t) = \left[\sum_{n=-\infty}^{\infty} A_n(t) * \delta\left(t - \frac{n}{\Delta\nu_s}\right)\right] e^{i\left[-2\pi\nu_1 t + \phi(t)\right]} + n(t), \tag{5}$$

where $A_n(t)$ is the amplitude of each pulse, $\phi(t)$ is random phase, and $n(t)$ is a wideband Gaussian process, which may be intrinsic to the pulsed source or a result of amplified

#167037 - $15.00 USD Received 18 Apr 2012; revised 25 Jun 2012; accepted 27 Jun 2012; published 3 Aug 2012

spontaneous emission (ASE) in subsequent optical amplification. After passing through the resonance, the field is given by $u_{in}(t)*t_g(t)$. Since we require that the convolved pulses do not overlap ($\tau_g \ll \nu_s^{-1}$), they can be individually analyzed via $u_n(t)=[A_n(t)e^{i[-2\pi\nu_1 t+\phi(t)]}]*t_g(t)$. Further assuming that $A_n(t)$ is limited to the pulse duration T_p, one obtains

$$u_{\mathrm{n}}(t)=t_g(t)\cdot\begin{cases}\int_0^t A_n(t')e^{i\phi(t')+t'/\tau_g}dt' & t<T_g\\ \int_0^{T_p} A_n(t')e^{i\phi(t')+t'/\tau_g}dt' & t\ge T_g,\end{cases} \tag{6}$$

Equation (6) shows that for times $t>T_p$ one obtains $u_n(t)=C_n t_g(t)$ where C_n is a complex constant. Thus, fluctuations in pulse amplitude or phase profile are converted to changes in the scale of $u_n(t)$, whereas its central frequency follows that of $t_g(t)$. Since $\tau_g \gg T_p$, the portion of $u_n(t)$ which exhibits fluctuations is small and becomes increasingly negligible as the resonance strength increases. In addition, the leading edge of $u_n(t)$ may be eliminated by actively modulating $u_n(t)$. As a result, detection schemes that are based on detecting frequency shifts in $u_n(t)$ may be unaffected by fluctuations in pulse phase or amplitude profiles as long as the pulse duration fulfills $\tau_g \gg T_p$. This property comes in stark contrast to both CW-interrogation techniques, where phase noise represents a fundamental limitation of the scheme. As a result, the additive wideband CW noise term may become a decisive factor in determining the detection sensitivity when narrow resonances ($\tau_g \gg T_p$) are considered. If the duration of $n(t)$ is reduced by gating to $T_n \ll \tau_g$, the noise can be analyzed using Eq. (6). In that case similarly to pulse fluctuations, the effect of $n(t)$ would become less dominant as the resonance strength is increased and may be eliminated by blocking the output for times $t<\mathrm{T}_P$.

3. Experimental results

3.1 Experimental setup

We experimentally tested the performance of the pulse-interferometry method for the transmission and reflection of a π-phase-shifted FBG. The experimental setups for the reflection and transmission measurements are shown in Figs. 2(a) and 2(b), respectively. Polarization maintaining fibers were used to maintain single polarization in all experiments. The source was a 90 fs laser with a repetition rate of 100 MHz, output power of 60 mW and spectral width of over 100 nm (Menlo Systems GmbH, Martinsried, Germany). In both schemes, frequency variations of the resonance were measured using an unbalanced MZ interferometer. Erbium-doped fiber amplifiers (EDFA) were used to amplify the signal after filtering. The MZ interferometer was stabilized to its quadrature point. Spectral inversion – a technique described in the Appendix in which the reflection spectrum is inverted and assumes the shape of the transmission spectrum – was performed using a Michelson interferometer stabilized to destructive interference on its output arm.. A computer generated feedback signal, fed into a piezo-electric fiber stretcher on one of the interferometer arms (Optiphase, Inc., Van Nuys, CA., USA) with a response bandwidth of 100 kHz, was used to stabilize both interferometers. The optical filter had a FWHM spectral width of 0.3 nm and was tuned to the frequency of the resonance. In all the experiments but the last, the detection bandwidth was set to 20 MHz. The FBG had a bandgap span of 1.38 nm and a FWHM resonance width of 8 pm, corresponding to a coupling coefficient ([43]) of $\kappa = 2.58\,\mathrm{mm}^{-1}$ and grating length of

#167037 - $15.00 USD Received 18 Apr 2012; revised 25 Jun 2012; accepted 27 Jun 2012; published 3 Aug 2012

$L = 2.38\,\mathrm{mm}$. According to the analysis presented in section 2.1, these values correspond to spectral-inversion efficiency of 0.66, as defined in the Appendix, i.e. the Lorentzian resonance constitutes 66% of the power of $i - r_g$.

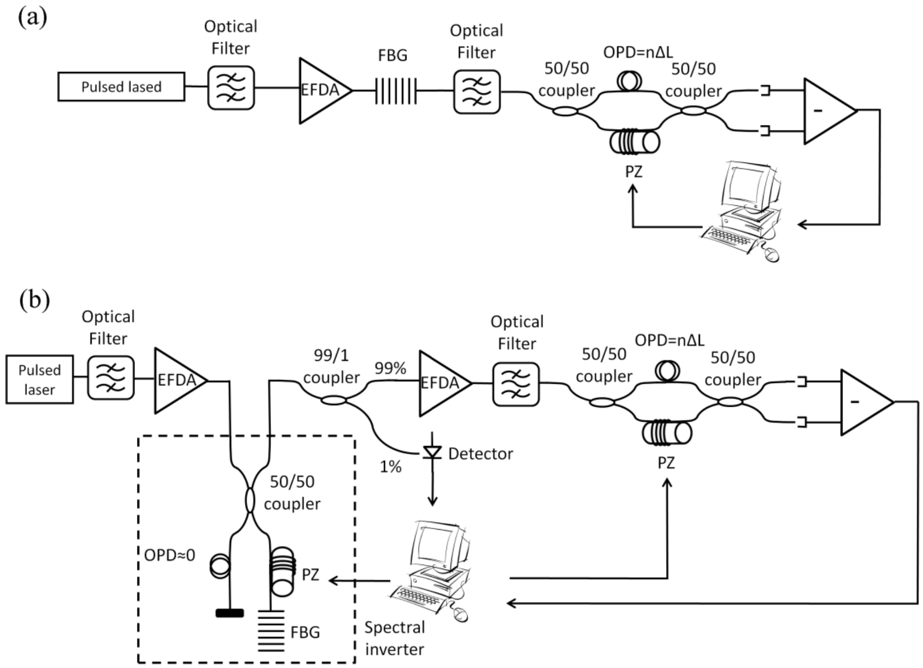

Fig. 2. The schematic of the system used for pulse-interferometry interrogation of a π-phase-shifted FBG in (a) transmission and (b) reflection. EDFA is erbium-doped fiber amplifier; OPD is optical path difference; PZ is piezo-electric element, and FBG is fiber Bragg grating.

In the first experiment, the performance of the spectral-inversion scheme was tested. For this, the MZ interferometer was not stabilized, but rather fed with a 25 Hz sinusoidal signal whose amplitude corresponded to phase shifts larger than 2π. Figures 3(a) and 3(b) show the differential signal at the output of the interferometer for transmission and reflection, respectively (solid-blue curves). The signals are also shown with the offset obtained when the measurement was performed for a single interferometer arm (dashed-red curves). For the transmission, the obtained visibility was 0.42, corresponding to an optical path delay (OPD) of approximately 8.1 cm. In the reflection, the visibility decreased to 0.27, corresponding to spectral-inversion efficiency of approximately 0.64. The spectral-inversion efficiency can be increased by improving the balance of the Michelson interferometer and by using a narrower, steeper optical bandpass filter. The high visibility obtained in the reflection measurement provides experimental proof of the spectral inversion. For comparison, when the mirror in the Michelson interferometer was removed, no visible interference was obtained in the reflection. Figure 3(c) shows transmission measurement with the source replaced by an ASE source.

3.2 Ultrasound detection

In the second experiment, the scheme was applied for broadband measurement of ultrasound fields. For this, a flat round ultrasonic transducer with a diameter of 6 mm (Model V323-SM, Olympus-NDT, Waltam, MA) was fed with 66 ns square electric pulse. The generated field was first measured by a pre-calibrated hydrophone (Model HPM1/1, Precision Acoustics Ltd., Dorset, U.K.) and was found to have a peak amplitude of approximately 175 kPa at a distance of 3.3 mm from the transducer's surface. The grating was then positioned in parallel to the transducer's axis at a similar distance. Because of the slow response of the feedback scheme, the fast resonance variations induced by the acoustic fields were not compensated for by the MZ interferometer stabilization, but were rather recorded by the differential signal at the output of the interferometer. Figure 3(d) shows the measured optical frequency shift of the resonance notch for the reflection (solid-blue curve) and transmission (dashed-red curve). As expected, the spectral inversion in the reflection measurement led to almost identical results in both measurements. Additionally, noise levels were similar in both experiments, and had a constant power spectral density in the ultrasound frequency band 100 kHz-20 MHz corresponding to a detection accuracy of 3.1 kHz/Hz$^{1/2}$ in the resonance shift. This value corresponds to the noise of a narrow-linewidth laser with $\Delta\nu_c = 31\,\text{MHz}$. In comparison, the noise level measured with the ASE source was 56 kHz/Hz$^{1/2}$.

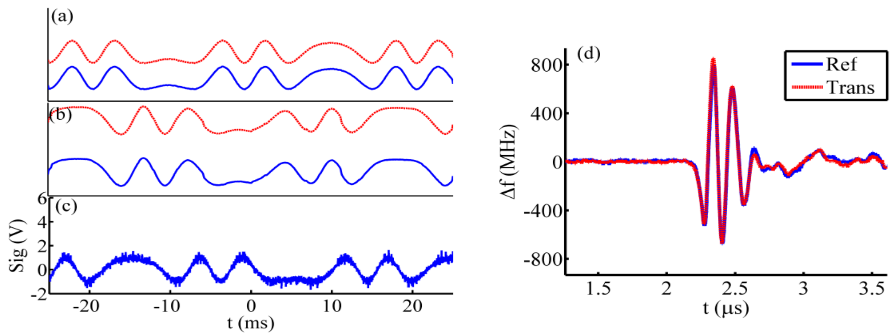

Fig. 3. (a-c) The output of the MZ interferometer when the optical path of one of the arms is modulated with a 25Hz sine signal. (a) transmission measurement with pulsed source; (b) reflection measurement with pulsed source achieved by spectral inversion; (c) transmission measurement with wideband CW source. The signals were obtained at the output of the differential detector (solid-blue curve), and are also presented with the offset obtained when the measurement was performed for a single interferometer arm (dashed-red curve). The higher SNR achieved by pulse-interferometry is clearly visible. The high visibility of the interference pattern in the reflection measurement reveals that spectral inversion of the reflection spectrum was achieved. (d) The grating response to an ultrasound wave with an approximate amplitude and duration of 175 kPa and 67 ns, respectively, obtained in reflection (solid-blue curve) and transmission (dashed-red curve). Because the inverted reflection spectrum follows the transmission, no meaningful difference was obtained between the two ultrasound measurements.

3.3 Noise properties

The third measurement aimed at analyzing the noise sources in the implementation of the pulse-interferometry scheme. Since the experimental setups shown in Fig. 2 involved optical amplifiers, the noise term $n(t)$ in Eq. (4) is expected. The experimental setup is shown in Fig. 4(a). The laser pulses propagated through the 0.3 nm optical bandpass filters into a MZ interferometer. The interferometer was stabilized to quadrature point while the noise and visibility were measured for different OPDs with 0.5 mm increments. The noise measurement was performed by calculating the standard deviation of the output voltage obtained over duration of 10 µs with 20 MHz bandwidth and was repeated with an ASE source replacing the pulse laser. Figure 4(b) shows the standard deviation of the photodiode's output as function of OPD for the laser (square-blue markers) and ASE (round-red markers) sources. At OPD = 0, the noise was similar for both cases, and was mostly a result of electronic noise. However, as the OPD was increased, optical noise became dominant in both cases. For better visualization of the results, in Fig. 4(c) the noise data is scaled to the same level and is presented with the measured interferometer's fringe visibility (dashed curve), which was identical for the two sources. We note that while the measured visibility is the same for CW and pulse interrogation, its underpinnings are different. In CW interferometry, visibility is determined

#167037 - $15.00 USD Received 18 Apr 2012; revised 25 Jun 2012; accepted 27 Jun 2012; published 3 Aug 2012

by the phase correlation between the two beams, whereas in pulse interferometry, it is determined by pulse overlap, where zero visibility indicates no overlap. Thus, for a pulsed source with $n(t) = 0$ (Eq. (5)), no interference noise should be obtained when the visibility vanishes. Nonetheless, the figure shows no decrease in noise for the case of the pulse laser as the visibility vanishes. Additionally, for both sources a similar trend is visible in the figure suggesting an ASE component in the pulse-interferometry setup.

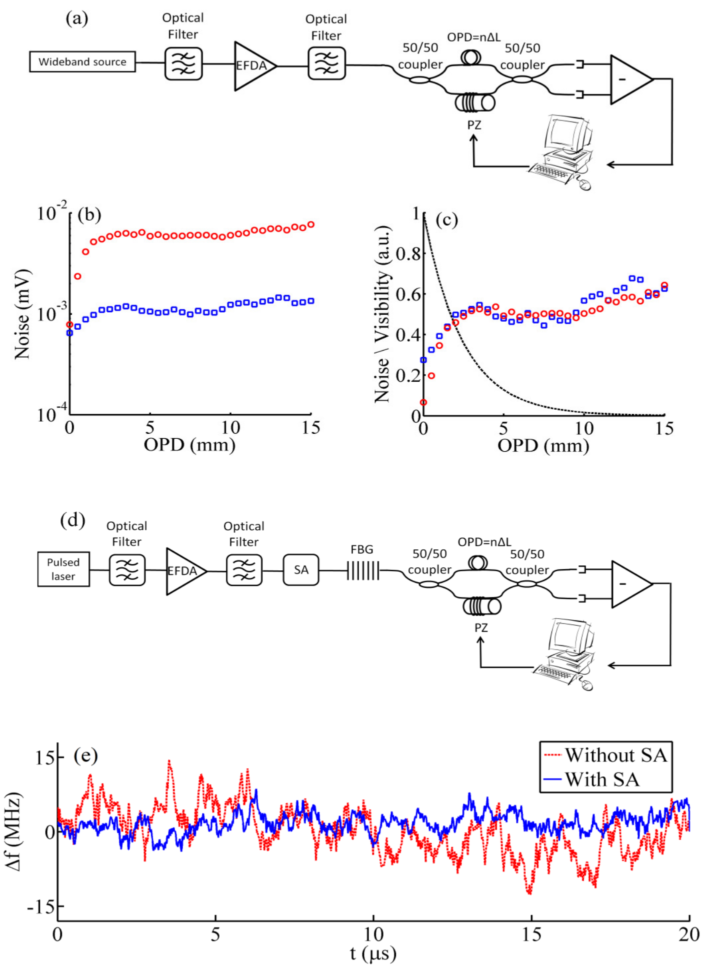

Fig. 4. (a) The schematic of the system used to evaluate the effect of ASE on the noise in the detection scheme. The visibility and noise level were measured for OPDs varying from 0 to 15 mm (b) The noise at the differential amplifier for wideband pulsed (blue square markers) and CW (red circle markers) sources as function of OPD obtained when the source is filtered to a bandwidth of 0.3 nm. The noise at OPD = 0 was mostly a result of electronic noise and was similar for both optical sources. (c) the noise data of Fig. 4(b) scaled to the same level for better visualization displayed with the measured fringe visibility (dashed curve). The similar dependency of noise for both cases indicates that the ASE noise is dominant in the pulse interferometry scheme. (d) The system used to test the effect of ASE rejection on noise reduction in the pulse interferometry setup. The saturable absorber (SA) added to the system had a transmission approximately 2.8 higher for the pulses compared to CW. (e) The noise recorded with the SA (solid-blue curve) and with an attenuator replacing the SA to ensure the same signal level (dashed-red curve). A reduction of 2.3 in the noise was observed, in correspondence with the SA rejection ratio.

#167037 - $15.00 USD Received 18 Apr 2012; revised 25 Jun 2012; accepted 27 Jun 2012; published 3 Aug 2012

In the last experiment, noise reduction is demonstrated through modulating the pulse train to reject the parasitic low-coherence CW component. The modulation is performed by adding a saturable absorber (SA) module to the transmission scheme, as shown in Fig. 4(d). The SA (Batop optoelectronics, Jena, Germany) exhibited an absorption resonance at the wavelength of the pulses, which corresponded to approximately 2.5% transmission at low power levels, whereas, for high input power, transmission of up to 45% could be achieved. The relaxation time constant of the module, i.e. the time required for the transmission state to change, was approximately 5 ps. According to the 0.3 nm bandwidth of the filters used, the estimated duration of the pulses was 26 ps. In our experiment, the input of the SA had a power of 23 mW, which lead to transmission of 7%, i.e. 2.8-fold increase compared to the low-power case. The recorded noise is shown in Fig. 4(e) for the SA case (solid curve) and attenuator case (dashed curve). The noise measured at the output of the MZ interferometer with the SA was 1.3 kHz/Hz$^{1/2}$, equivalent to the noise level of narrow-linewidth interrogation with $\Delta\nu_c = 6\,\text{MHz}$. This noise level represents a 2.3-fold improvement over the results obtained for pulse interferometry without ASE rejection and a 40-fold improvement in comparison to low-coherence interferometry.

4. Discussion and conclusions

In this paper, a new method for wideband interrogation of optical sensors is demonstrated and suggested as an alternative to conventional coherent (narrow linewidth) and incoherent (wideband) CW interrogation. The method is based on a pulse laser source whose bandwidth is significantly broader than the resonance width of the sensor and on inteferometric demodulation. The use of a wideband coherent source opens new possibilities for interrogation methods with an advantageous combination of properties that cannot be found in conventional CW methods. Specifically, pulse interferometry could enable the use of passive demodulation techniques, which do not require stabilization, and performing parallel multiplexing with a single source while potentially offering sensitivity levels comparable to standard coherent CW methods. To evaluate the performance of the technique, it was experimentally tested for interrogating a single resonator with active demodulation with a MZ interferometer locked to quadrature. However, the interferometer stabilization was only against low frequency disturbances, whereas the ultrasound signal was measured as the deviation of the interferometer from quadrature, limiting the maximum amplitude ultrasound which can be measured. This property also appears in PDH techniques, which are also not stabilized at ultrasound frequencies. Nonetheless, for the sensor studied in this work, it has been previously found that ultrasound amplitudes approaching 1 MPa may be measured without being significantly distorted [10]. When a higher dynamic range is sought, passive demodulation may be used in pulsed interferometry. In contrast, a higher dynamic range in PDH methods would require a faster response of the locking mechanism.

Our theoretical and experimental results indicate that the limiting factor for sensitivity in the current implementation of pulse interferometry is the parasitic incoherent CW signal accompanying the pulses. By using a saturatable absorber for rejecting the parasitic signal, sensitivity comparable to a 6 MHz linewidth CW laser was achieved. This sensitivity is 40 times higher than that achieved in this work for incoherent CW interferometry. As the main noise source is optical, a similar sensitivity level is expected in passive-demodulation implementations of the technique. Further sensitivity enhancement may be achieved via improvements in the ASE-rejection scheme. Ultimately and similarly to CW techniques, the sensitivity of pulse interferometry is limited by shot noise.

In addition to the sensitivity increase over incoherent CW interferometry, we also address the general incompatibility of wideband interrogation techniques with reflection-mode sensing of optical resonators. This trait, which is not characteristic to coherent CW interferometry, would have been a major limitation for the practical application of pulse interferometry for sensing since in some applications, e.g. catheters and endoscopes, the sensor is only accessible from one side. To overcome this drawback, a new technique termed spectral inversion is introduced. A designated experimental setup performs the inversion by destructively interfering the reflection from the resonator with a reference signal reflected from a mirror. The result is an inverted spectrum whose shape is identical to that of the transmission. In contrast to the case of transmission measurement, spectral inversion can be performed only with active stabilization, necessitating a stabilized feedback system. The required gain-bandwidth product of the feedback system is however determined by the fluctuations in the difference between the optical paths leading to the resonator and reference mirror and not by resonator itself. As a result, proper shielding of the fibers – excluding the sensor – as well as bundling the fibers together to minimize the difference in environmental conditions could significantly reduce the required performance of the stabilization system. In contrast, in coherent CW interferometry, the required gain-bandwidth product of the stabilization system depends only on the resonance width and the environmental conditions perceived by the sensor itself. In that case, weakening the requirements for the stabilization system can only be done when using sensors with broader resonance (and thus weaker signal) or, alternatively, by desensitizing the sensor's response to environmental conditions, which may however lead to reduced sensitivity.

Currently, the main drawbacks of pulse interferometry are the cost and complexity associated with pulsed lasers, which are significantly higher than those of distributed-feedback lasers commonly used in PDH-based schemes. However, since pulse interferometry is a wideband technique, it readily lends itself to wavelength division multiplexing with a single source. In the case studied in this work, in which the sensor is a π-phase-shifted FBG, the laser's bandwidth is sufficient for multiplexing a typical number of 100 resonators in a single fiber. If several fibers are used, the total number of sensors could reach thousands. Such multiplexing capabilities are important in the field of medical ultrasound, where sensor arrays with over 100 elements are already commonplace. When considering these figures, the realization of a sensor array depends almost exclusively on the complexity and cost of the components which need to be scaled with the number of detectors, making the relatively high cost of a single femtosecond laser less relevant. In the case of transmission mode, a trivial generalization of the technique described in this work would require that the number of MZ stabilized interferometers photodetectors be scaled with the number of sensors. However, the use of techniques such as carrier modulation [2] and frequency division multiplexing [27] may significantly reduce the number of these components. In comparison, in PDH the number of lasers must be scaled with the number of detectors. Arguably, the biggest challenge in multiplexing pulse-interferometry systems would be devising techniques for wideband ASE rejection. The ASE-rejection technique used in this work is not easily scalable as the SA had a relatively narrow operational bandwidth. Additionally, in multiplexing implementations, there might be a need for more amplification stages, which might also contribute to the ASE.

APPENDIX

π-phase-shifted fiber-Bragg gratings

An FBG is a semi-harmonic perturbation of the effective refractive index of the core of an optical fiber usually characterized by its modulation amplitude n_{ac}, nominal period Λ, phase $\theta(z)$ and length L [43]. An ideal π-phase-shifted FBG is characterized by $n_{ac}(z) = n_{ac}$ and $\theta(z) = \pi U(z - L/2)$, where U is the Heaviside step function. In this case, the central frequency of the grating is given by $\nu_0 = c(2n_0\Lambda)^{-1}$, c, n_0, being the velocity of light in vacuum, and the effective refractive index of the fiber, respectively. The reflection and transmission spectra of π-phase-shifted FBGs can be analytically approximated around the resonance using the transmission-matrix method [10, 43], i.e.

#167037 - $15.00 USD Received 18 Apr 2012; revised 25 Jun 2012; accepted 27 Jun 2012; published 3 Aug 2012

$$r_g(k) \cong \frac{k}{2\kappa e^{-\kappa L} - ik} \quad (7)$$

$$t_g(k) \cong \frac{2i\kappa e^{-\kappa L}}{2\kappa e^{-\kappa L} - ik}, \quad (8)$$

where $k = -2\pi n_0(\nu - \nu_0)/c$ and $\kappa = \pi/(2n_0\Lambda)n_{ac}$ fulfill $k \ll \kappa$ and $\kappa L \gg 1$ and ν denotes optical frequency. Thus, the intensity transmission of the defect-mode resonance has a Lorentzian shape with a full-width-at-half-maximum (FWHM) bandwidth of $\Delta\nu = 2c\kappa \exp(-\kappa L)/(n_0\pi)$. From Eqs. (7) and (8) it follows that $t_g \cong i - r_g$; thus, the reflection spectrum can be inverted to yield the transmission spectrum if it is interfered with a wave of constant phase. In order to perform the spectral inversion, the illumination frequencies should be limited to a range over which Eqs. (7) and (8) are valid. For $2\kappa\exp(-\kappa L) \ll |k| \ll \kappa$, we obtain $i - r_g = k/\kappa + O[(k/\kappa)^2]$. By Fourier transforming Eq. (1), the impulse response of the grating resonance is obtained: $t_g(t) = i\tau_g^{-1}\exp(-t/\tau_g - 2\pi i\nu_0 t)U(t)$ where $\tau_g = n_0(2\kappa e^{-\kappa L}c)^{-1}$ is the effective time during which light is trapped in the resonance. Thus, in sensing applications, the bandwidth of the sensor equals $\Delta\nu$.

#167037 - $15.00 USD Received 18 Apr 2012; revised 25 Jun 2012; accepted 27 Jun 2012; published 3 Aug 2012